OXFORD UNIVERSITY PRESS | Aesthetic Surgery Journal

Beyond the L-strut: Redefining the biomechanics of rhinoplasty using topographic optimization modeling

Journal:	*Aesthetic Surgery Journal*
Manuscript ID	ASJ-18-0500.R1
Manuscript Type:	Special Topic
Subject Collection:	Rhinoplasty
Keywords:	L-strut, finite element modeling, topographical optimization modeling, rhinoplasty, septal failure, Cartilage graft < OCULOPLASTICS
Abstract:	Rhinoplasty utilizes cartilage harvested from the nasal septum as autologous graft material. Traditional dogma espouses preservation the "L-strut" of dorsal and caudal septum which is as less resistant to axial loading than virgin septum. With the 90° angle between dorsal and caudal limbs the traditional L-strut also suffers from localized increases in internal stresses leading to premature septal 'cracking', structural-scale deformation or both. Deformation and failure of the L-strut leads to nasal deviation, saddle deformity, loss of tip support or restriction of the nasal valve. The balance between cartilage yield and structural integrity is a topographical optimization problem. Guided by finite element (FE) modelling, recent efforts have yielded important modifications including the chamfering of right-angled corners to reduce stress concentrations and the preservation of a minimum width along the inferior portion of the caudal strut. However, all existing FE studies make simplified assumptions to make the construct easier to model. This review article highlights advances in our understanding of septal engineering and identifies areas that require more work in order to further refine the balance between the competing interests of graft acquisition and the maintenance of nasal structural integrity.

Abstract

Rhinoplasty utilizes cartilage harvested from the nasal septum as autologous graft material. Traditional dogma espouses preservation the "L-strut" of dorsal and caudal septum which is as less resistant to axial loading than virgin septum. With the 90° angle between dorsal and caudal limbs the traditional L-strut also suffers from localized increases in internal stresses leading to premature septal 'cracking', structural-scale deformation or both. Deformation and failure of the L-strut leads to nasal deviation, saddle deformity, loss of tip support or restriction of the nasal valve. The balance between cartilage yield and structural integrity is a topographical optimization problem. Guided by finite element (FE) modelling, recent efforts have yielded important modifications including the chamfering of right-angled corners to reduce stress concentrations and the preservation of a minimum width along the inferior portion of the caudal strut. However, all existing FE studies make simplified assumptions to make the construct easier to model. This review article highlights advances in our understanding of septal engineering and identifies areas that require more work in order to further refine the balance between the competing interests of graft acquisition and the maintenance of nasal structural integrity.

Introduction

Aesthetic and reconstructive rhinoplasty utilizes autologous septal cartilage to fashion grafts for aesthetic and functional modifications [1]. The residual cartilaginous construct is often referred to as an "L-strut" with preservation of the dorsal and caudal septum [2]. Cartilage yield is variable and does not readily correlate with external nasal projection [3]. Historically, the default position was to take as much as possible. However, the nasal septum supports the lower two-thirds of the nose. Moreover, cartilage is a mechanosensitive tissue and mechanical deformation ("warping") or failure of the L-strut leads to adverse aesthetic and functional consequences including nasal collapse, saddle deformity, tip deviation and nasal blockage which can be difficult to manage secondarily [4]. Increasing awareness of septal biomechanics has led surgeons to acknowledge the need to balance the competing interests of cartilage yield with nasal stability. In biomechanics, this topographical optimization problem can be solved with a model built with sufficient data to reflect the variables involved. The variables considered in analytical models of this problem include the geometry of the L-strut, the material properties of septal hyaline cartilage, boundary conditions of the nasal septum and adjacent soft tissue support [5–7]. While a number of studies have sought to define one or more of these variables they assume a linear-elastic material constitutive law for the septal hyaline cartilage, adopt imprecise descriptions of boundary conditions and assume idealized loading vector at the nasal tip. Hence, the complete picture remains elusive. The specific goals of this review are to:

(1) Describe the biomechanical behavior of the nasal septum in relation to its composition and boundary conditions.

(2) Describe the modes of typical failure in virgin and "L-strut" septum and the biomechanical implications of septal failure

(3) Describe the science of septal harvest biostructural optimization, define the current limitations and anticipate future refinements

As the geometry of septal cartilage preservation is surgically controllable, this review forms the basis for the mathematical optimization of septal graft harvest through finite element (FE) modeling.

Part I. Biomechanics of the nasal septum

The nasal septum is thought to play a crucial role in mid-facial growth and development [8,9]. It may also serve as a vertical strut, supporting the midface against masticatory loading [10] and providing a platform for the alveolar arch. Moreover, the nasal septum plays an important role in tip support at its caudal end and may provide stress-absorption in facial trauma [11]. Loss of structural integrity of the dorsal septum results in saddle nose deformity and airway obstruction while loss of structural integrity of the caudal septum at the anterior or posterior angle results in loss of tip support [4,12]. Surgical modification of the septal cartilage provides autologous graft material for nasal aesthetic and functional modification, alters nasal projection and relieves turbulent airflow at the level of the valve.

Septal topography

The nasal septum exhibits considerable topographic heterogeneity with the septal base and cranial regions being the thickest [13–15]. The thinnest areas incorporate part of the traditional L-strut including the anterior septal angle [13,14]. Compositional analysis of human septal cartilage revealed no age or gender variations in hydration or collagen content but sulfated glycosaminoglycan (sGAG) content and cell number decreased with increasing age [16,17]. Region-specific variation exists, with higher levels of collagen in the caudal region and higher levels of sGAG in the ventral region and the highest ratio of collagen to sGAG in the dorsal region [18]. This region-specific compositional variation is summarized in **figure 1**. The nasal septum also exhibits considerable anatomic variation at the osseocartilaginous junction with a variable and

anatomically indistinct border between the posterior extent of the quadrilateral cartilage and the perpendicular plate of the ethmoid [19].

Material properties of septal hyaline cartilage

Glycosaminoglycans bestow cartilage with its compressive properties while type II collagen and elastins provide tensile and flexural strength. In general, the complex relationships between collagen structure, fibril elasticity, and mechanical response are not yet well understood. What is clear is that septal cartilage exhibits remarkably complex material behavior featuring aspects of nonlinear stress–stretch responses, anisotropy (where different mechanical properties are observed in different material orientations), viscoelasticity (the exhibition of both viscous and elastic components in material deformation) and poroelasticity (the interaction between the elastic solid and fluid components in material deformation) in the context of large deformations with negligible volume changes. Under displacement-controlled uniaxial tension, nasal cartilage exhibits a stress-stretch response that comprises 3 regions. Region 1 is a low stiffness toe region of approximately constant stiffness which occurs at very small strains. Region 2 occurs at higher strains (up to 20% nominal strain) where the gradient increases rapidly due to reorientation of the collagen fibers towards the direction of loading causing it to stretch. Region 3 involves tensile stretching of the collagen fibers (this leads to tearing and/or plastic deformation if the stretch is sufficiently large) leading to progressive softening and, ultimately, failure by material separation [20,21]. Typical material properties obtained from a uniaxial tensile test include its modulus of elasticity (or Young's modulus), Poisson's ratio and tensile strength [20]. The Young's modulus measures the resistance of a material to being deformed elastically, typically at small strains.

Poisson's ratio, by contrast, describes the ratio of transverse contraction strain to longitudinal extensional strain in the direction of the stretching force. However, the (typically) small sample specimen, coupled with a large variability in their mechanical properties and their complex collagenous structure, makes it difficult to ascertain whether or not the properties measured are affected by size- effects [22] and can lead to wrong estimated values for the parameters in the constitutive equations [23]. Moreover, fresh specimens are favored owing to demonstrable changes in the material properties by storage and preparation [24]. The compressive and flexural strength of septal cartilage are also commonly reported by performing constrained compression and 3-point bending tests, respectively [24,25].

For the purpose of examining the material properties of hyaline septal cartilage as a source of autologous graft material, the most commonly used measurements are tensile, compressive and flexural strength and Young's modulus. The aforesaid parameters are generally sufficient to define a linear-elastic constitutive model for use in FE models of the traditional "L-strut" to identify regions of high stress concentration. However, they are insufficient to model, and capture, the complex fracture patterns observed in septal fracture [19] without invoking the concept of internal variables (through continuum damage mechanics) to describe the softening response, irreversible effects and subsequent material separation, that occurs in Region 3 of its stress-stretch response.

Human septal cartilage has been shown to exhibit tensile isotropy (same tensile strength in all orientations) [20] but compressive anisotropy [25], with greater compressive stiffness in the vertical

and cranial-caudal axes than the medial axis. This may reflect collagen fiber orientation and has important implications for stress relaxation on load direction and rate. Additionally, it has been demonstrated that adjacent perichondrium exhibits high tensile strength [26] and influences Young's modulus [12,27]. Neither donor age nor gender have been found to significantly influence tensile strength or material compression [20,25]. In a model of a sustained load, human native and cultured septal cartilage has been found to exhibit a high degree of shape fidelity [28]. Chondrocyte viability has been found to be inversely proportional to the degree of crush, an important consideration when reshaping harvested graft material [29].

Boundary conditions of the nasal septum

The boundary of the quadrangular cartilage includes the perpendicular plate of the ethmoid cranially, the maxillary crest inferiorly, the vomer posteriorly and the nasal bone cap dorsally which may overlap the central keystone (K) area by up to 14mm [30]. The lower lateral cartilages and associated ligamentous attachments form additional support caudally. The existing FE models in literature assume, for simplicity, rigid osseocartilaginous boundaries hence a clear delineation between the two constituents (cartilage and bone), i.e. a 'fully-clamped' boundary in structural engineering terminology. In reality, the boundary condition is more akin to a functionally graded material (or FGM) with a continuously-graded variation of composition, porosity, and possibly internal microstructure, over the bulk material – leading to local variations in mechanical properties across the material space that bridges the osseocartilaginous boundary. The result is a compliant, as opposed to an ideal rigid, boundary with no clear demarcation between cartilage and nasal bone. The exact nature on why and how the osseocartilaginous

boundary evolves to become functionally graded is unclear. However, existing applications of FGM in materials engineering typically arises from a need to achieve a set of incompatible mechanical functions during performance optimization trade-offs [31].

Part II. Septal failure

Deformation and failure of virgin septum

Patterns of traumatic failure of the virgin septum yield important information about the influence of septal topography, the material properties of septal cartilage and the boundary conditions on the biostructural integrity of the nasal construct. Typically, traumatic failure of the nasal septum occurs either in parallel to the maxillary crest (a fracture of Jarjavay) or perpendicular to the maxillary crest (a fracture of Chevallet) (**figure 2**). The former is associated with force applied to the nasal dorsum while the latter is associated with a laterally applied force. More rarely, the septal failure pattern is termed "C" or "S" shaped. As testimony to the strength of the osseocartilaginous junction, fractures are not typically encountered in this area [32]. The relationship between attritional stress and mechanical deformation (warping) in virgin septum remains unexamined. As mechanical engineers recognize several forms of warping (including bowing, twisting, kinking, cupping and crooking) insights into how virgin septum deforms in response to repetitive stress is a crucial step towards our understanding of biostructural integrity.

Deformation and failure of the L-strut

In 1905 Killian noted that preservation of the dorsal and caudal aspects of the quadrilateral septal cartilage (the L-strut) ensured a stable upper lateral cartilage and anterior projection of the nose (**figure 3**) [2]. Two additional structural elements provide the support to the L- strut itself. The first is the septal lining flap and the second is the overlap with the bony vault. Increasing overlap with the bony vault has been shown to control the stability of the L-strut itself, as has the design of the segment that overlaps. A common rule is to preserve 10 – 15mm of width in order to

maintain septal biomechanical integrity, but these values owe more to tradition than empirical data [4]. The clinical evidence shows this to be a flawed concept with up to 40% of secondary cases showing fractures near the anterior septal angle [33]. The patterns of L-strut failure observed during surgical correction of primary rhinoplasty include vertical fracture, horizontal fracture (or a component of the two) and warping. Examples of these are shown in **figure 4**.

Biomechanical implications of loss of L-strut integrity

Anderson's tripod theory of nasal biomechanics asserted that tip projection resulted from an equilibrium between three pilar structures (the two lower lateral cartilages and the upper lateral cartilage) [34]. Janeke and Wright proposed that the nasal tip was supported by four key ligamentous structures; the ligamentous attachment of the upper and lower nasal cartilages, the attachment of the lateral crus to the pyriform aperture, the ligamentous attachment of the paired domes of the lower lateral cartilages and the attachment of the medial crura to the posterior caudal septum [35]. Recent evidence however shows there is no ligament between the medial crura and the septum while an intercrural ligament does exist [36]. Tardy and colleagues postulated that the nasal tip was supported by major and minor structural components relating these components to the anatomical failures of primary rhinoplasty [37]. Subsequent finite element modelling (FEM) demonstrated statistically significant correlations between these mechanical failures and the supporting subunits [38,39]. Further evidence for the importance of the arrangement of suspensory ligaments is demonstrated by the fact that disruption of the ligamentous attachments in the dome between the intermediate crura and between the medial crura leads to nasal tip collapse, suggesting that nasal tip projection is partly achieved through a

tightly controlled suspension system anchored through ligamentous attachments at the alar scroll area and the upper lateral cartilages and between the alar cartilages strung over the vertical Pitanguy ligament. Rather than the concept of a fixed tripod or major and minor mechanisms, the nasal tip could be a finely controlled suspension bridge [36]. While these theories have helped to explain surgical failures, avoiding the loss of projection of the nasal tip has proven to be more difficult.

The anatomy of the virgin nose is a complex interplay of multiple tissue types. The upper nasal vault is formed by the bony structures of the ethmoid, maxillary and nasal bones covering the septum and upper laterals for a variable length. The lower nasal vault is constructed from the upper lateral cartilages, the nasal septum-embryologically all the same cartilage but in which clefts may be present and the lower lateral cartilages. The latter neatly balanced on the former. Superiorly the upper lateral cartilages form the bony cartilaginous junction extending under the nasal bone 'cap' and further cranially is the spine of the frontal bone and perpendicular plate of the ethmoid. Anatomical variations between these cartilaginous and bony structures result in variation of the shapes of the nasal dorsum

Part III. L-strut optimization using finite element modeling

Existing models

Mau et al. [5] produced a simplified finite element model of Killian's L-strut (**figure 5A**). A four sided rectangular cartilage shape was used to investigate the L-strut and two modifications to the L-strut geometry. They concluded that the preservation of a triangular piece of cartilage at the dorsal anchor (the bony cartilaginous junction) enhanced the maximal tensile stress accommodated at the bony cartilaginous junction [5]. The model assumed a homogeneous linear-elastic cartilage of uniform thickness. Moreover, it did not take into account the boundary conditions including tip support by the adjacent lower lateral cartilages [40] and only two modifications were investigated. Lee et al. [6] developed a more complex finite element (FE) model (**figure 5B**). In their case the shape was based on the quadrilateral cartilage. The values for tensile and compressive elastic moduli and Poisson's ratio were based on the work of Grellman et al and Richmon et al [20,24,25]. Both free and spring supported nasal tip models were used. They found that the points of maximal stress were the bony cartilaginous junction and the nasal spine. Narrowing the dorsal strut resulted in an increase in the maximal tensile stresses at the BC junction while the inclusion of an arc of cartilage at the dorsal anchor decreased maximal stress. As expected, the spring supported tip model resulted in much lower maximal stresses but also exhibited a different pattern of deformation, with a gentle curving of the dorsal septum. For the purpose of their model, they too assumed that the material properties of septal cartilage were homogeneous, linearly elastic and of uniform thickness.

More recently, Lee et al. [7,41] developed FE modeling to investigate stress and strain patterns on the L-strut by varying the boundary conditions (the contact between the caudal strut and the maxillary crest) . In this model, the load was applied to the dorsal limb of the L-strut at various points along its length instead of at the nasal tip. The model accommodated variations in the thickness of the L-strut cartilage according to their background data. They established that, as expected, the internal L-strut angle was a point of relatively high stress. They further demonstrated that the stress increased as contact between the caudal L-strut and the maxillary crest diminished and, in conclusion, suggested that preservation of at least 1cm width of contact between the caudal L-strut and the anterior nasal spine was necessary (**figure 5C**) [41]. In the second study, they concluded that as the greatest stress occurred in the inferior caudal L-strut, this area must either be reinforced or preserved and that dorsal onlays should avoid placing stress on the supratip breakpoint as pressure here causes the greatest stress to the construct (**figure 5D**) [7].

Limitations of existing models

All of the above studies assume a clear demarcation between cartilage and nasal bone, with an idealized rigid boundary provided by the latter to the former, as opposed to a functionally-graded boundary in reality. Because of the linear-elastic constitutive assumption, valid only for reversible deformation at small strains, it cannot model the mechanical behavior of septal cartilage with damage arising from non-physiological loads, such as tearing and plastic deformation of the collagen fibers that occur at larger strains; consequently, none of the FE models would be suitable for use to optimize cartilage yield.

Another major problem with existing FE models is assumed isotropy of septal cartilage, a material that is known to be anisotropic. Thus, FE models using viscoelastic data derived from homogenous, denuded cartilage will incorporate observational errors into the model. Moreover, the clinical implications of material anisotropy are, as yet, unclear particularly with reference to load bearing grafts such as the columellar strut graft.

Published FE studies adopt a linear-elastic constitutive assumption, requiring only the Young's modulus and Poisson's ratio as input parameters. Whilst they may be successful in helping to determine, and eliminate, hot-spot stresses in the traditional "L-strut", they are incapable of modeling failure (and fracture patterns) that occur under large deformation, which have implications on the long-term stability of the nasal structure. Two issues exist: first, the Young's modulus is typically obtained from the toe-region and is only valid at small strains; second, a physically-based constitutive model of the septal cartilage that accounts for damage initiation, damage evolution and its subsequent failure (material separation leading to total loss of load carrying capacity) is lacking.

The earliest constitutive models to describe the material behavior of soft biological tissues mainly utilized phenomenological equations to relate the deformation to the stress state of the tissue. The advantages of this approach are that the results are relatively straightforward to interpret and it represents a computationally-efficient method to describe material responses. On the other hand, it is often difficult to assign a physiological meaning to material parameters, which complicates any interpretation in terms of biological mechanisms. There are a number of recent

developments on microstructurally-motivated constitutive models [42–47] that would allow one to delve deeper into the physical and biological principles of material behavior. In addition, the use of multiscale modeling is likely to be inevitable when attempting to capturing phenomena occurring at different spatial and temporal scales. In short, an accurate constitutive model is needed to optimize cartilage yield whilst ensuring structural compromises to the "L-strut" remain within acceptable limits.

Part IV: Future directions: beyond the L-strut

Elucidating the complex relationships between collagen structure, fibril elasticity, and mechanical response

An accurate constitutive model of the stress–stretch response that includes both microstructural and tissue level aspects of the structural hierarchy in its formulation, coupled with damage, is still lacking for septal cartilage. At the microstructural scale, a constitutive law for collagen fibers must be derived based on strain-energy formulation. The three-dimensional orientation and deformation of the collagen fibrils that aggregate to form fibers has to be taken into consideration through some form of probability distribution function. Moreover, the contribution of the inorganic matrix to hydrostatic stresses must be taken into account. At the tissue level, an average stress versus stretch relation would need to be computed by assuming a statistical distribution for fiber straightening during tissue loading. Again, a probability distribution function must be prescribed for the distribution of fiber straightening stretch. This approach would allow the resulting comprehensive stress–stretch law to be experimentally calibrated (at different scales) for the unknown parameters, which will represent structural and microstructural organization, fibril elasticity, as well as a failure criterion (either stretch or strain

based). There are recent developments in the coupled anisotropic damage modeling of fibrous soft tissues that consider separated contributions on damage from the matrix and fibers in soft biological tissue by Calvo et al. [46] and Gasser & Holzapfel [47] which will be applicable here; collectively, these works, coupled with careful experimentation to calibrate unknown model parameters, lay the mathematical foundation needed to describe structural damage in septal cartilage. Additionally, understanding the material properties of septal cartilage are necessary to develop tissue-engineered alternatives [18,48].

Boundary conditions

The predictive accuracy of a FE model is contingent on an accurate description of the boundary conditions. The actual boundary conditions of the nasal septum is a functionally-graded construction and is much more complex than has yet been appreciated by a topographic model. Moreover, it is, as yet, unclear how composition, porosity, and possibly internal microstructure varies across cartilage and nasal bone and this will require further investigations. FE modeling would be useful to achieve a better understanding of the interplay between the nasal tip and associated support structures [38,39].

Loading and failure

Failure, both in virgin and operated septum, may occur as a consequence of major energy transfer (such as an axial or laterally-delivered blow to the external nose). However, equally interestingly from the point of view of FE modeling is the influence on the septum of the attritional effects of daily living including repeated deformation by minor forces such as the

dynamic compressions of the nasal musculature rubbing and blowing. Loading by the centripetal redistribution of cartilage from the center to the dorsal or caudal areas of the nose if the support line of the lower 2/3 is not respected will lead to long term failure. As the final arbiter of an FE model is the ability to accurately predict the patterns of failure observed in reality, we must learn more about how attritional deformation and failure manifests.

A topological optimization problem

The balance between obtaining sufficient septal cartilage to execute the surgical plan while preserving biostructural integrity must be formulated as a topological optimization problem. Topological optimization is a mathematical method typically used to optimize material layout within a given design space, for a set of loads, boundary conditions, material properties and constraints with the goal of maximizing performance (in this case, the structural stability of the nose following the harvest of septal cartilage). We have shown that, while simplified finite element models have suggested modifications to the traditional L-strut, current models lack sufficient detail on each of the variables necessary to be able to tackle the problem authoritatively or make predictions on deformation and failure *in vita reali*.

Limitations of this study

Our proposed model looks at a well understood problem in a different way and proposes a different set of tools to reach an answer that is clinically meaningful. However, a mathematical model is only as accurate as the data on which it is based. We have highlighted a number of areas where the experimental data are inadequate, including the material properties of human nasal

septal cartilage and attritional (as well as traumatic) deformation and failure of the virgin septum. Thus, a number of complex investigations are necessary to yield data to populate the model. Additionally, what this paper highlights above all else is that the surgical manipulation of the nasal septum has the potential to compromise the biostructural integrity of the nose and the corollary of this is that rhinoplasty surgeons must seek to embrace the concept of biostructural preservation in their surgical planning.

Summary

Finite element modeling has yielded important insights into the structural integrity of the nasal septum with the goal of maintaining shape fidelity after rhinoplasty. As these models become more sophisticated, they are changing the way we think about the design of what we leave behind after septal cartilage harvest. It is thus time to move away from the concept of the L-strut (except in reconstructive rhinoplasty) and towards biostructural optimization. While important modifications have already been made, existing models rely on assumptions and simplifications. In redefining the parameters of the model, we can exploit an almost unique opportunity in surgical science; to solve a clinical problem with a topographical optimization model.

References

1. Nahai F. *The Art of Aesthetic Surgery: Principles and Techniques (2nd. Ed.)*. CRC Press; 2011.
2. Killian G. The submucous window resection of the nasal septum. *Ann Otol Rhinol Laryngol*. 1905;14:363-93.
3. Kim J, Khan NA, Jang YJ. Intraoperative Measurements of Harvestable Septal Cartilage in rhinoplasty. *Ann Plast Surg*. 2010;65(6):519-523.
4. Kim DW, Gurney T. Management of naso-septal L-strut deformities. *Facial Plast Surg*. 2006;22(1).
5. Mau T, Mau S-T, Kim DW. Cadaveric and engineering analysis of the septal L-strut. *Laryngoscope*. 2007;117(11):1902-6.
6. Lee SJ, Liong K, Tse KM, Lee HP. Biomechanics of the deformity of septal L-struts. *Laryngoscope*. 2010;120(8):1508-1515.
7. Lee JS, Lee DC, Ha DH, Kim SW, Cho DW. Redefining the septal L-strut to prevent collapse. *PLoS One*. 2016;11(4):e0153056. doi:10.1371/ journal.pone.0153056 Editor.
8. Scott JH. The cartilage of the nasal septum. *Br Dent J*. 1953;95:37-43.
9. Harvey Kemble J V. The importance of the nasal septum in facial development. *J Laryngol Otol*. 1973;87(4):379-386.
10. Al Dayeh AA, Rafferty K., Egbert M, Herring SW. Deformation of nasal septal cartilage during mastication. *J Morphol*. 2009;270(10):1209-18.
11. Lee SJ, Liong K, Lee HP. Deformation of nasal septum during nasal trauma. *Laryngoscope*. 2010;120(10):1931-1939.

12. Westreich RW, Courtland H-W, Nasser P, Jepsen K, Lawson W. Defining Nasal Cartilage Elasticity. *JAMA Facial Plast Surg*. 207AD;9(4):264-270.

13. Hwang K, Huan F, Kim DJ. Mapping Thickness of Nasal Septal Cartilage. *J Craniofac Surg*. 2010;21(1):243-244.

14. de Pochat VD, Alonso N, Figueredo A, Ribeiro EB, Mendes RRDS, Meneses JVL. The role of septal cartilage in rhinoplasty: cadaveric analysis and assessment of graft selection. *Aesthetic Surg J*. 2011;31(8):891-6.

15. Mowlavi A, Masouem S, Kalkanis J, Guyuron B. Septal Cartilage Defined: Implications for Nasal Dynamics and Rhinoplasty. *Plast Reconstr Surg*. 2006;117(7):2171-2174.

16. Homicz MR, McGowan KB, Lottman LM, Beh G, Sah RL, Watson D. A Compositional Analysis of Human Nasal Septal Cartilage. *Arch Facial Plast Surg*. 2003;5:53-58.

17. Rotter N, Tobias G, Lebl M, et al. Age-related changes in the composition and mechanical properties of human nasal cartilage. *Arch Biochem Biophys*. 2002;403(1):132-140.

18. Neuman MK, Briggs KK, Masuda K, Sah RL, Watson D. A compositional analysis of cadaveric human nasal septal cartilage. *Laryngoscope*. 2013;123(9):2120-2124.

19. Lee M, Inman J, Callahan S, Ducic Y. Fracture patterns of the nasal septum. *Otolaryngol - Head Neck Surg*. 2010;143(6):784-788.

20. Richmon JD, Sage AB, Wong VW, et al. Tensile biomechanical properties of human nasal septal cartilage. *Am J Rhinol*. 19(6):617-22.

21. Guo B yun, Liao D hua, Li X yang, Zeng Y jun, Yang Q hua. Age and gender related changes in biomechanical properties of healthy human costal cartilage. *Clin Biomech*. 2007;22(3):292-297.

22. Odom EM, Adams DF. Specimen size effect during tensile testing of an unreinforced polymer. *J Mater Sci*. 1992;27:1767-1771.

23. Sacks MS. Incorporation of Experimentally-Derived Fiber Orientation into a Structural Constitutive Model for Planar Collagenous Tissues. *J biomech Eng*. 2003;125(2):280-87.

24. Grellmann W, Berghaus A, Haberland E-J, et al. Determination of strength and deformation behavior of human cartilage for the determination of sugnificant parameters. *J Biomed Mater Res*. 2006;78:168-74.

25. Richmon JD, Sage A, Wong VW, Chen AC, Sah RL, Watson D. Compressive biomechanical properties of human nasal septal cartilage. *Am J Rhinol*. 2006;20(5):496-501.

26. Kim DW, Egan KK, O'Grady K, Toriumi DM. Biomechanical strength of human nasal septal lining: comparison of the constituent layers. *Laryngoscope*. 2005;115(8):1451-3.

27. Roy R, Kohles SS, Zaporojan V, et al. Analysis of bending behavior of native and engineered auricular and costal cartilage. *J Biomed Mater Res A*. 2004;68(4):597-602.

28. Reuther MS, Briggs KK, Neuman MK, Masuda K, Sah RL, Watson D. Shape fidelity of native and engineered human nasal septal cartilage. *Otolaryngol - Head Neck Surg (United States)*. 2013;148(5):753-757.

29. Cakmak O, Buyuklu F, Yilmaz Z, Sahin FI, Tarhan E, Ozluoglu LN. Viability of cultured human nasal septum chondrocytes after crushing. *Arch Facial Plast Surg*. 2005;7(6):406-9.

30. Palhazi P, Daniel RK, Kosins AM. The osseocartilaginous vault of the nose: Anatomy and surgical observations. *Aesthetic Surg J*. 2015;35(3):242-251.

31. Birman V, Byrd LW. Modeling and Analysis of Functionally Graded Materials and

Structures. *Appl Mech Rev*. 2007;60(5):195.

32. Harrison DH. Nasal Injuries: Their pathogenesis and treatment. *Br J Plast Surg*. 1979;32:57-64.

33. East C, Kwame I, Hannan SA. Revision Rhinoplasty: What Can We Learn from Error Patterns? An Analysis of Revision Surgery. *Facial Plast Surg*. 2016;32(4):409-415.

34. Anderson JR. A reasoned approach to nasal base surgery. *Arch Otolaryngol Neck Surg*. 1984;110(6):349-58.

35. Janeke J., Wright WK. Studies on the support of the nasal tip. *Arch Otolaryngol Neck Surg*. 1971;93(5):458-64.

36. Daniel RK, Palhazi P. The Nasal Ligaments and Tip Support in Rhinoplasty: An Anatomical Study. *Aesthetic Surg J*. 2018;38(May):357-368.

37. Tardy ME, Brown R. *Surgical Anatomy of the Nose*. New York, NY: Raven Press; 1990.

38. Manuel CT, Leary R, Protsenko DE, Wong BJF. Nasal tip support: A finite element analysis of the role of the caudal septum during tip depression. *Laryngoscope*. 2014;124(3):649-654.

39. Shamouelian D, Leary RP, Manuel CT, Harb R, Protsenko DE, Wong BJF. Rethinking nasal tip support: A finite element analysis. *Laryngoscope*. 2015;125(2):326-330.

40. Westreich RW, Lawson W. The tripod theory of nasal tip support revisited: the cantilevered spring model. *Arch Facial Plast Surg*. 2008;10(3):170-9.

41. Lee J, Lee DC, Ha DH, Kim SW. Redefining the Septal L-Strut in Septal Surgery. *PLoS One*. 2015;10(3):e0119996. doi:10.1371/ journal.pone.0119996.

42. Farquar T, Dawson P., Torzilli PA. A Microstructural Model for the Anisotropic Drained

Stiffness of Articular Cartilage. *J biomech Eng*. 1990;112(4):414-25.

43. Hurscher C, Loitz-Ramage B, Vanderby R. A structurally based stress-stretch relationship for tendon and ligament. *J biomech Eng*. 1997;119:392-99.

44. Alastrué V, Rodríguez JF, Calvo B, Doblaré M. Structural damage models for fibrous biological soft tissues. *Int J Solids Struct*. 2007;44(18-19):5894-5911.

45. Rodriguez J, Cacho F, Bea J, Doblare M. A stochastic-structurally based three dimensional finite-strain damage model for fibrous soft tissue. *J Mech Phys Solids*. 2006;54:564-86.

46. Calvo B, Pena E, Martinez MA, Doblare M. An uncoupled directional damage model for fibred biological soft tissues. Formulation and computational aspects. *Int J Numer Meth Engng*. 2007;69:2036-57.

47. Gasser TC, Holzapfel GA. A rate-independent elastoplastic constitutive model for biological fiber-reinforced composites at finite strains: Continuum basis, algorithmic formulation and finite element implementation. *Comput Mech*. 2002;29(4-5):340-360.

48. Zemek A, Garg R, Wong BJF. Model for estimating the threshold mechanical stability of structural cartilage grafts used in rhinoplasty. *Laryngoscope*. 2009;120(6):1089-1093.

Figure 1: The material composition of the nasal septum (from Neuman et al 2013) [18], demonstrating region-specific compositional variation with higher levels of collagen in the caudally, higher levels of sulfated glycosaminoglycans (sGAG) ventrally and the highest ratio of collagen to sGAG dorsally.

Figure 2: Failure patterns of the virgin septum secondary to trauma. **A:** The fracture of Jarjavay which lies roughly parallel to the maxillary crest propagating towards perpendicular plate of the ethmoid. This fracture is typically caused by the absorption of force in an AP direction. **B:** The fracture of Chevallet which lies roughly perpendicular to the maxillary crest. This fracture is typically caused by the absorption of force in a lateral direction.

Figure 3: Killian's traditional L-strut (1905) [2].

Figure 4: Examples of L-strut failure ascertained by secondary rhinoplasty. **A:** A vertical fracture at the L-strut angle in a 25 year old woman. **B:** Combination fracture and warping in a 32 year old man. **C:** a horizontal fracture at the L-strut angle, in the same 32 year old man.

Figure 5: Existing finite element models of L-strut structural optimization. **A:** From Mau et al (2007) [5], demonstrating enhanced maximal tensile stress at the dorsal anchor with increased dorsal limb contact. **B:** From Lee et al (2010)[6], using free and spring-supported nasal tip models to demonstrate the points of maximal tensile stress. These models confirmed the earlier observation that maximal tensile stress could be enhanced with increased dorsal limb contact. **C:**

From Lee et al (2015)[41], investigating stress at the L-strut angle with changing boundary conditions and a dorsally applied force. This model demonstrated increased stress at the L-strut angle when contact between the caudal limb and the maxillary crest was reduced. **D:** From Lee et al (2016)[7], a refinement of the previous model demonstrating how the tensile stress on the caudal limb varied with the placement of the dorsally applied force.

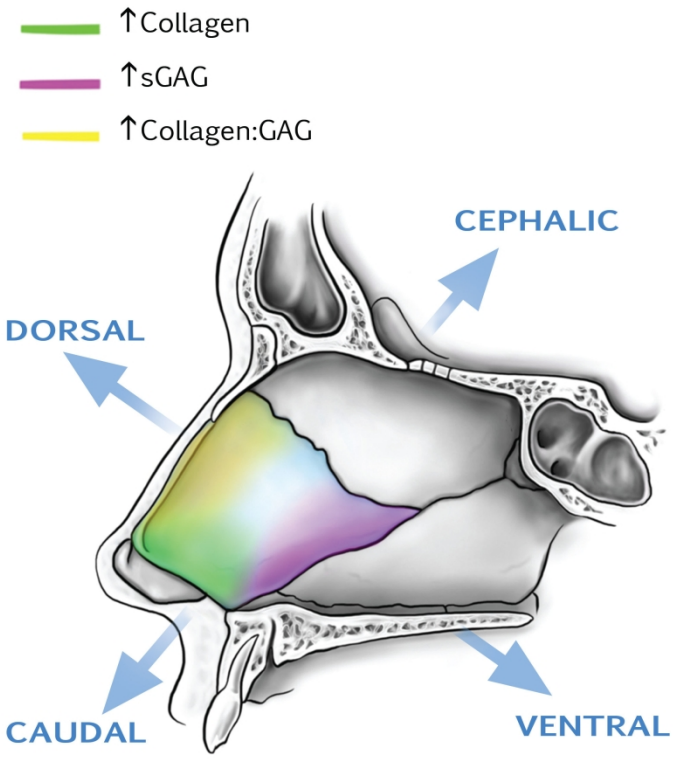

Figure 1: The material composition of the nasal septum (from Neuman et al 2013) 18, demonstrating region-specific compositional variation with higher levels of collagen in the caudally, higher levels of sulfated glycosaminoglycans (sGAG) ventrally and the highest ratio of collagen to sGAG dorsally.

209x297mm (300 x 300 DPI)

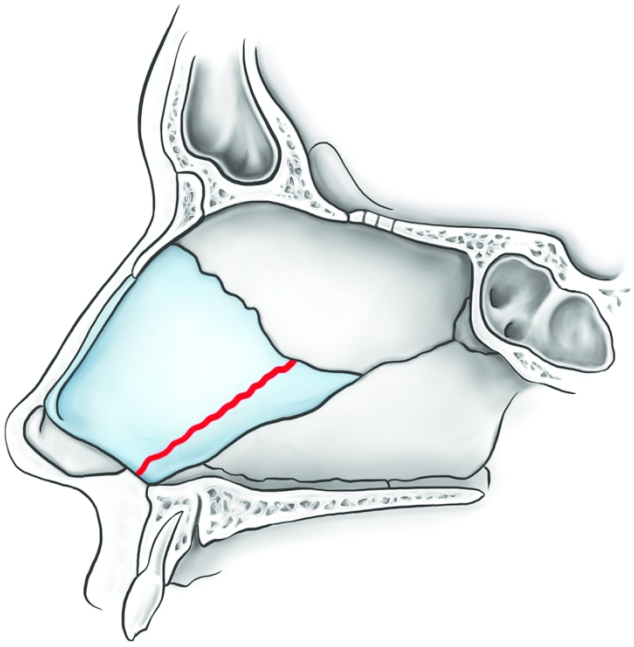

Figure 2: Failure patterns of the virgin septum secondary to trauma. A: The fracture of Jarjavay which lies roughly parallel to the maxillary crest propagating towards perpendicular plate of the ethmoid. This fracture is typically caused by the absorption of force in an AP direction.

209x297mm (300 x 300 DPI)

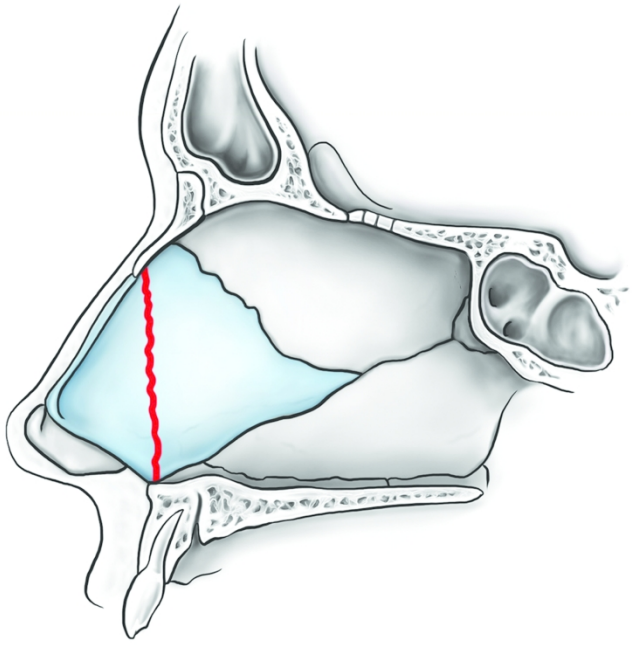

B: The fracture of Chevallet which lies roughly perpendicular to the maxillary crest. This fracture is typically caused by the absorption of force in a lateral direction.

209x297mm (300 x 300 DPI)

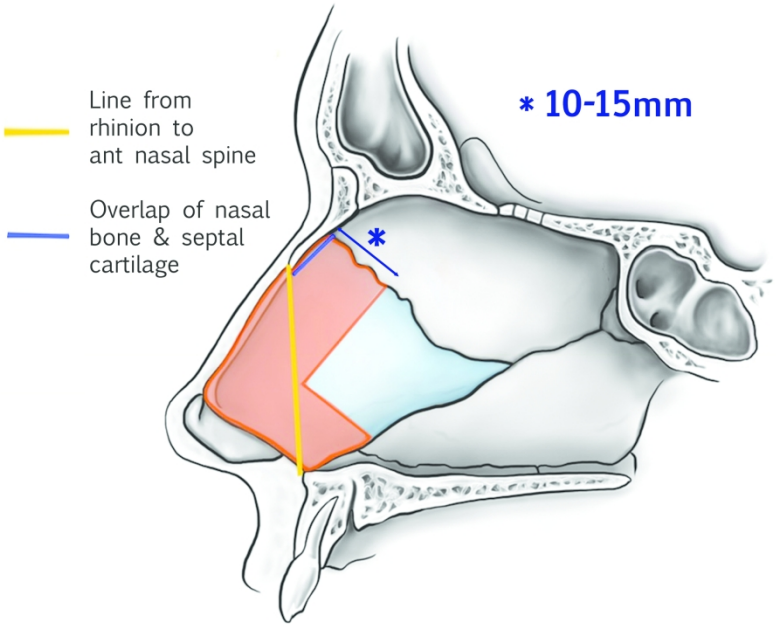

Figure 3: Killian's traditional L-strut (1905) 2.

209x296mm (300 x 300 DPI)

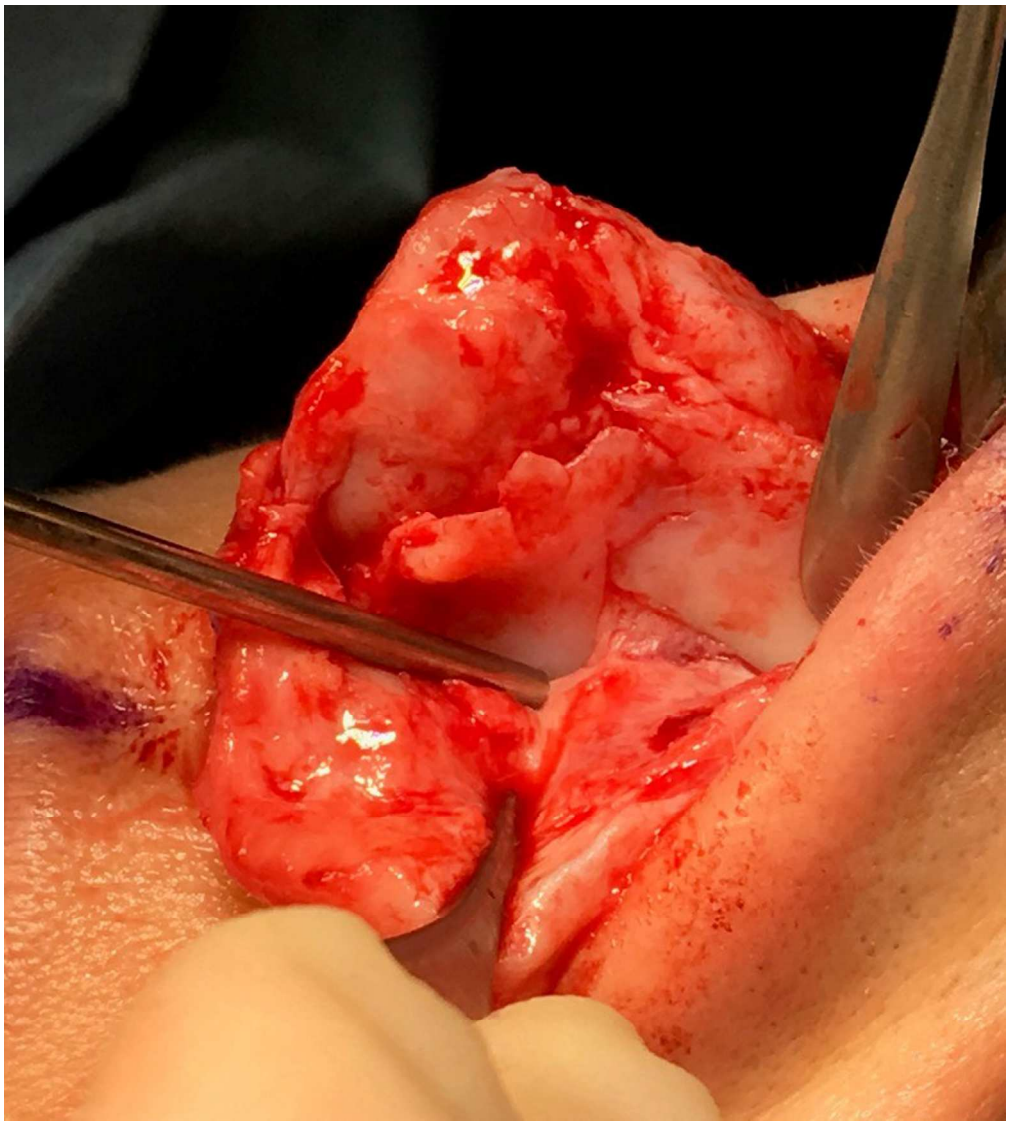

Figure 4: Examples of L-strut failure ascertained by secondary rhinoplasty. A: A vertical fracture at the L-strut angle.

296x330mm (72 x 72 DPI)

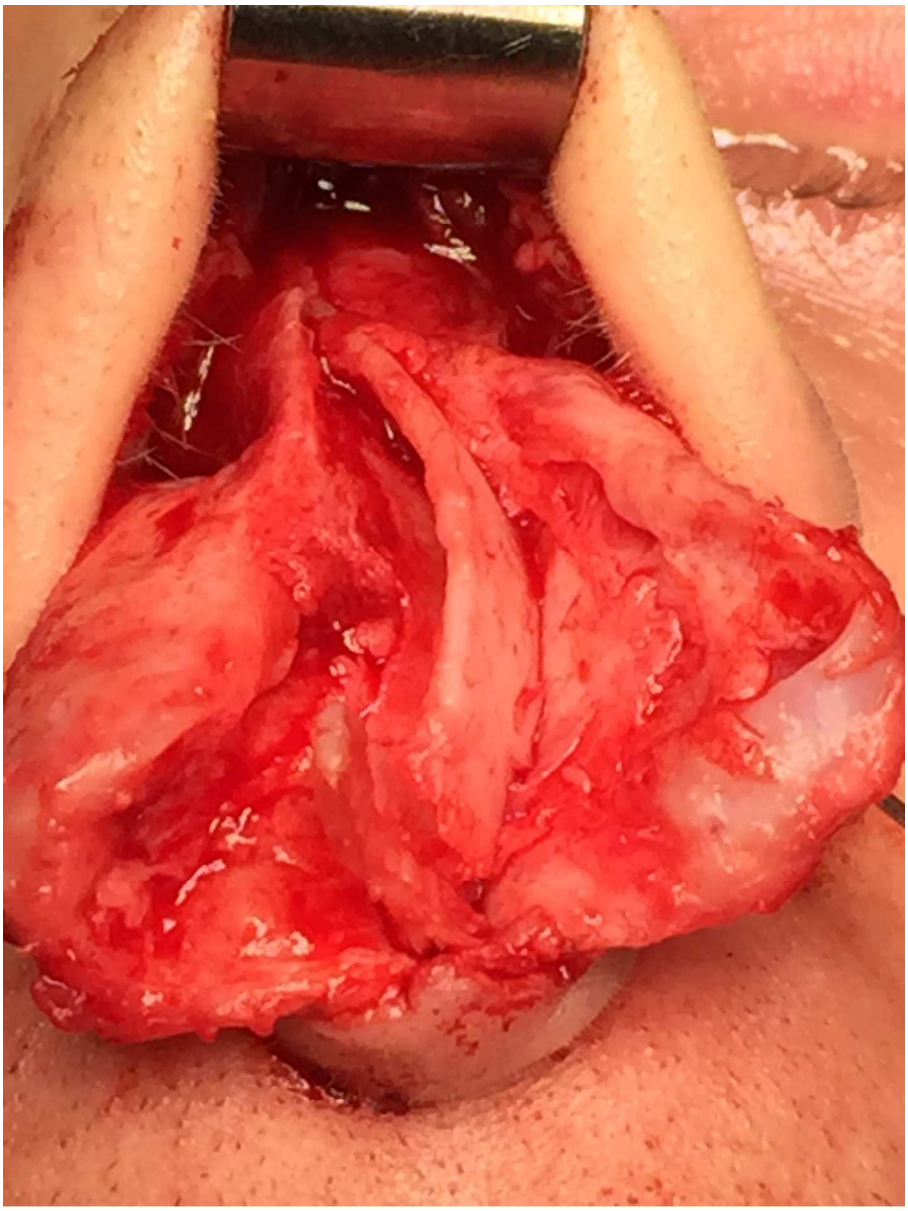

Figure 4B: Combination fracture and warping.

863x1151mm (72 x 72 DPI)

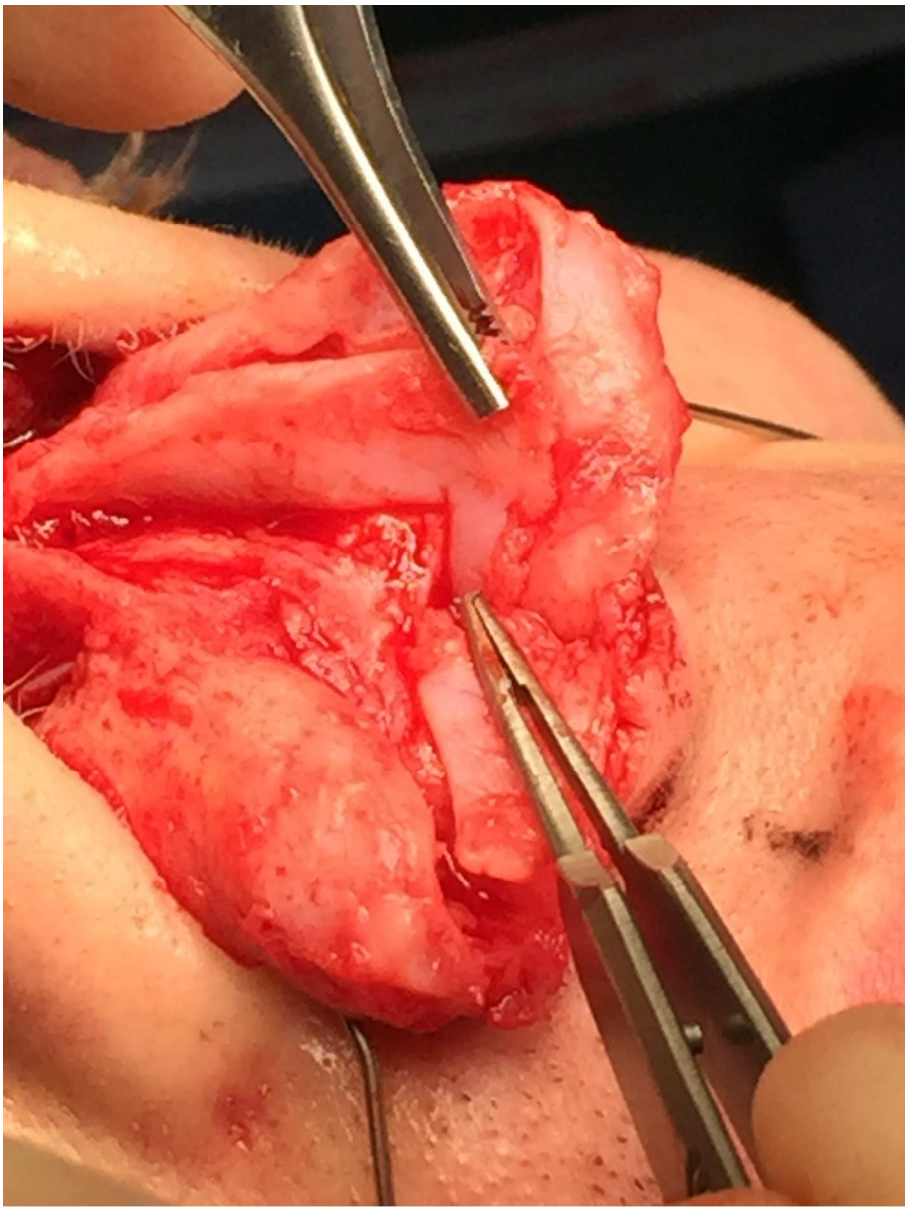

Figure 4C: a horizontal fracture at the L-strut angle.

863x1151mm (72 x 72 DPI)

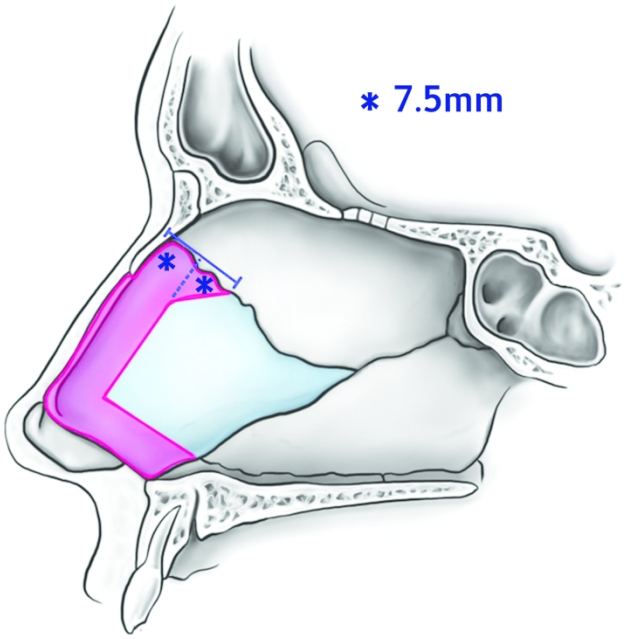

Figure 5: Existing finite element models of L-strut structural optimization. A: From Mau et al (2007) 5, demonstrating enhanced maximal tensile stress at the dorsal anchor with increased dorsal limb contact.

209x296mm (300 x 300 DPI)

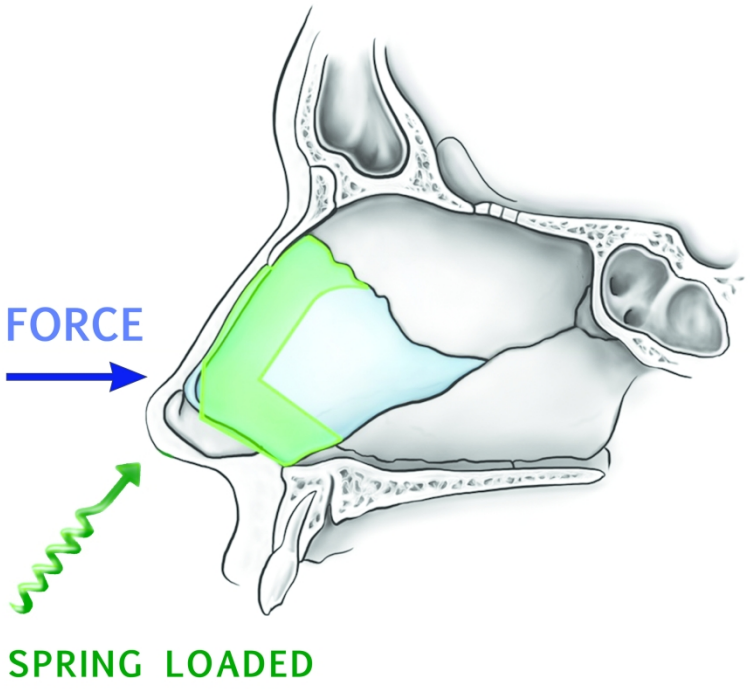

B: From Lee et al (2010)6, using free and spring-supported nasal tip models to demonstrate the points of maximal tensile stress. These models confirmed the earlier observation that maximal tensile stress could be enhanced with increased dorsal limb contact.

209x296mm (300 x 300 DPI)

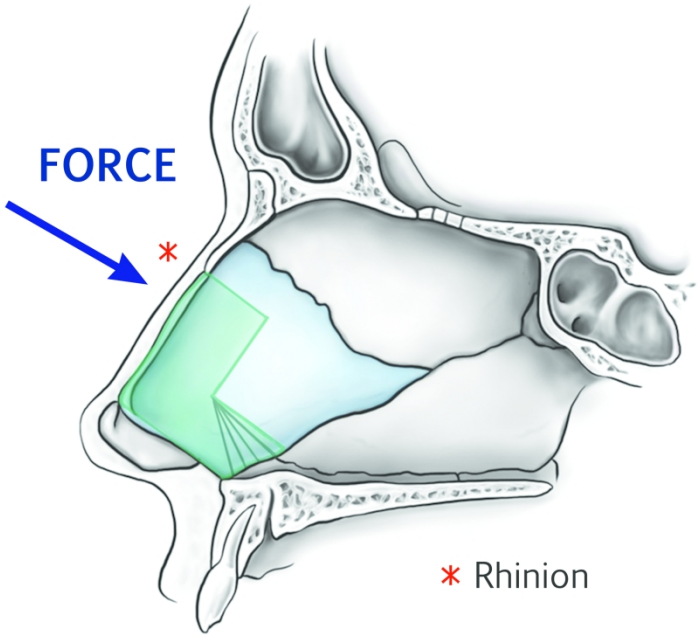

C: From Lee et al (2015)41, investigating stress at the L-strut angle with changing boundary conditions and a dorsally applied force. This model demonstrated increased stress at the L-strut angle when contact between the caudal limb and the maxillary crest was reduced.

209x296mm (300 x 300 DPI)

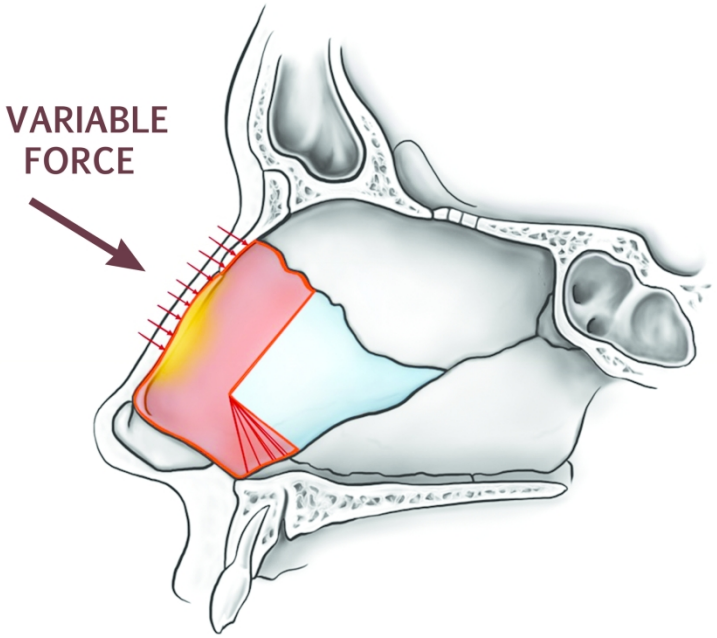

D: From Lee et al (2016)7, a refinement of the previous model demonstrating how the tensile stress on the caudal limb varied with the placement of the dorsally applied force.

209x296mm (300 x 300 DPI)